Sustainable Chemical Engineering
https://ojs.wiserpub.com/index.php/SCE/

UNIVERSAL WISER PUBLISHER

Research Article

Photocatalytic Oxidation of Benzene to Phenol and Dye Over N and S Doped Ferromagnetic Nanosize TiO_2

Madhavi Shete*, Julio Fernandes

Department of Chemistry, Goa University, Taleigao, Goa, India
E-mail: smadhavi91@gmail.com

Received: 27 July 2023; **Revised:** 24 August 2023; **Accepted:** 30 August 2023

Abstract: In the present investigation, we report the presence of N, S, and Ti^{3+} in the TiO_2 samples, and the surface exhibits acidic characteristics. The synthesized TiO_2 samples were also found to be ferromagnetic at room temperature and show higher photocatalytic activity compared to commercially available TiO_2 (DP-25). Nano-sized TiO_2 with a high surface area was obtained through a simple sol-gel synthesis method, using hydrazine sulfate as fuel during synthesis. The synthesized TiO_2 was found to contain N and S doping, with surface defects present due to cationic and anionic vacancies. The presence of defects was confirmed by Raman spectroscopy, infrared (IR) spectroscopy, scanning electron microscopy with energy-dispersive X-ray spectroscopy (SEM-EDAX), and photoluminescence (PL) analysis. The presence of Ti^{3+} in the TiO_2 samples was confirmed by Electron Spin Resonance spectroscopy (ESR) and X-ray Photoelectron Spectroscopy (XPS). XPS also revealed nitrogen and sulfur doping in the TiO_2 samples. The synthesized TiO_2 possesses an acidic surface, and surface acidity was measured through pyridine adsorption and ammonia-Temperature-Programmed Desorption (NH_3-TPD) studies. The ferromagnetic behavior of the synthesized samples was confirmed by Vibrating Sample Magnetometer (VSM) measurements. The synthesized samples were further studied for their photocatalytic activity in methylene blue dye degradation, 4-nitrophenol degradation, and photo-oxidation of benzene to phenol. We report the synthesis of TiO_2 with simultaneous nitrogen and sulfur doping, exhibiting ferromagnetism and high activity toward photocatalytic oxidation reactions.

***Keywords*:** defects, ferromagnetism, magnetic moment, adsorption

1. Introduction

A good photocatalyst semiconductor should possess high band gap properties. TiO_2 is one of the metal oxide semiconductor with a high band gap and acts as a good photocatalyst. TiO_2 is well known as a semiconductor photocatalysts due to its high band gap which is an important property for semiconductor to act as photocatalyst. TiO_2 mainly exists in three phases anatase, rutile and brookite. The most commonly studied phases of TiO_2 in photocatalysis are the anatase and rutile phases. Since Anatase has a high band gap (Eg = 3.2 eV) and in anatase, TiO_2 has less possibility for the electron-hole (e^--h^+) recombination thus mostly preferred as photocatalyst while rutile (Eg = 3.0 eV) phase is the most stable phase. Photocatalytic properties are dependent on physicochemical variables such as particle size, pore volume, surface area, and crystallanity. Other than surface area, the crystallanity and activity of TiO_2 are also

DOI: https://doi.org/10.37256/sce.4220233450

dependent on the morphology, therefore soft template synthesis of mesoporous anatase TiO_2 nanosphere was synthesized and found to have enhanced photocatalytic activity.[1] TiO_2 with acidic surface is found to be a more photocatalytically active material. Suphation and desulphated TiO_2 are found to have with higher acidic surface character than the other synthesized TiO_2.[2-3] Sulphation in TiO_2 leads to an increase in the acidity and also gives TiO_2 with high surface area with an anatase phase whereas desulphation during the synthesis may result in the formation of the vacancies thus altering its photocatalytic activity.[1] The presence of surface oxygen deficiencies can act as capture centers for the photoexcited electrons and holes, while the surface hydroxyl group acts as centers for the photocatalytic reaction. Oxygen defects are located in the vicinities of the rutile-anatase border. In terms of energy, these oxygen vacancy states in the anatase were determined to be located 2.02-2.5 eV above the valence band and the band gap corresponds to wavelength 506-614 nm. Besides other properties hydrophilicity in TiO_2 also enhances the rate of photocatalysis by undergoing self-cleaning process.[4] The presence of pollutants such as organic dyes and phenols in the waste water has become one of the crucial problems and to overcome this photo-oxidation is the most convenient process. Photo-oxidation processes by using semiconductors as photocatalyst are well known and TiO_2 as photocatalyst is preferred mainly due to its favourable properties like non-toxicity, chemical inertness, and stability over a wide pH range.

Photocatalytic activity usually depends on the surface properties such as surface area, surface acidity and presence of other impurities and defects.[5-8] One of the potential solutions for improving the efficiency of TiO_2 is to shift its absorption from UV region into the visible light region, allowing for more photons to be adsorbed and utilized in decomposing the pollutants. TiO_2 with Ti^{4+} oxidation state usually shows the least activity in the visible light due to a large band gap of 3.2 eV as compared to Ti^{3+}. In Ti^{4+} the electron-hole pair energy levels are larger to absorb large amounts of visible light more efficiently. In order to overcome this limitation, it's necessary to have reduced TiO_2 containing Ti^{3+} to be a visible light active photocatalyst. Apart from Ti^{3+}, TiO_2 with nitrogen and sulphur doping also shows visible light activity by altering their band gap and energy levels.[9] Doping of the nitrogen and sulphur shortens the TiO_2 band gap thus electrons in the conduction bands are easily available for the reduction to take place when irradiated with the light Presence of oxygen vacancies and Ti^{3+} introduces ferromagnetism in the TiO_2. It is interesting to know that Ti^{3+} ions with one 3d electron are usually generated in slightly reduced TiO_2. In such case, oxygen is removed and the excess electrons are unpaired and can occupy nearby localized Ti 3d orbit and therefore convert Ti^{4+} ions to Ti^{3+} ions.[10] The presence of oxygen vacancies on the surface of TiO_2 plays an important role in the adsorption of the O_2 producing superoxide species, O_2^-. Adsorbed O_2^- will later react with a photogenerated hole resulting in the desorption of O_2 (g) and forming an oxidizing agent in the photocatalytic process.[11] It is well known that ferromagnetism exists in the TiO_2 thin films.[12] Such ferromagnetism exists in the nanorod and films due to high surface area which possesses abundant surface defects.

Our present attempt is to synthesize N and S doped nanposize TiO_2 with high surface area to investigate room temperature ferromagnetism and its activity towards photocatalysis.

We herein report the synthesis of ferromagnetic N and S doped TiO_2 and the effect of the surface defect and acidity of catalyst on photocatalytic activity. In the present study we have used hydrazine sulphate as fuel during the synthesis and the following synthesis is carried out by simple sol-gel method. In comparison to the hydrazine sulphate another TiO_2 was also synthesized by using ammonium sulphate as fuel. We investigate the surface, optical and magnetic properties of the synthesized TiO_2 in order to study particle size, surface area, band gap and origin of ferromagnetism in the samples.

The samples with small particle size, high surface area and presence of Ti^{3+} could have led to enhanced ferromagnetism at room temperature. The use of hydrazine sulphate during the synthesis has led to the incorporation of nitrogen and sulphur into the lattice thus showing high photocatalytic activity in the sunlight. Incorporation of the nitrogen and sulphur in the TiO_2 will change its band gap to smaller values by altering its energy levels thus due to the smaller band gap electron are easily available in the conduction band for the reduction to take place when it is irradiated with light. Thus showing high photocatalytic activity. In the present investigation it will be studied that synthesized TiO_2 exhibits a highly reactive surface with nitrogen, sulphur and Ti^{3+} species. Surface is also acidic and has ferromagnetic behavior at room temperature and such reactive samples are further studied for their photocatalytic activity by selecting two pollutants methylene blue and 4-nitrophenol. The production of phenol is an important industrial process due to its high demand in the manufacturing of very important polymers, including polyamides, polycarbonates and phenolic resins. Phenol was obtained primarily from coal tar in small amounts.[13] The hock process was later developed to obtain

phenol from cumene through the intermediate formation of hydroperoxide and giving acetone as a co-product. Direct oxidation of benzene was also carried out by using N_2O on a zeolite catalyst, but the use of nitrous oxide involves the formation of adipic acid and also requires a purification step to remove various nitrous oxides and oxygen.[13] Although there are also other processes to obtain phenol these still involve difficulties either in the number of steps in the process or in purification of the product. Therefore there is a need for developing a suitable green method for the synthesis of phenol.

A photocatalytic process constitutes a greener approach to obtaining industrially important compounds such as phenol, in the presence of an environmentally safe oxidant such as H_2O_2. Recently photocatalytic phenol production was carried out by direct oxidation of benzene using Au-Pd metal nanoparticles supported on TiO_2.[14] Ambient oxidation of benzene to phenol was carried out on V-doped TiO_2 under UV irradiation. Higher catalytic activity was observed on a gold-supported catalyst. The enhanced activity was attributed to the presence of the Schottky junction due to metal doping thus altering the band energy levels, mesoporosity and charge carriers. The highest % conversion of benzene to phenol was 18%. For the comparative study between the synthesised TiO_2 and DP-25 photooxidation of benzene to phenol was carried out. Further properties of the synthesized samples and reactivity compared with reference to commercial DP-25 sample.

2. Chemical synthesis

TiO_2 was synthesized by using Titanium isopropoxide as the Ti precursor and Hydrazine sulphate. Hydrazine sulphate was dissolved separately in a minimum quantity of distilled water and to that titanium, isopropoxide was added at 0 °C such that the final molar composition of Titanium isopropoxide to hydrazine sulphate was 1:2 and 1:3 was stirred for 2 h. The resulting solution was dried at 70 °C thus forming a white color precursor. Thermal analysis of the dried precursor was carried out and further precursor was calcined at 600 °C for 3 h to give final TiO_2 samples as T1 and T. Similarly another TiO_2 was synthesized by using Titanium isopropoxide and ammonium sulphate and its code is T2.

2.1 *Catalyst characterization*

Phase identification was carried out from X-ray powder diffraction of the patterns (XRD) recorded on a Rigaku Ultima IV diffractometer, using Ni filtered Cu Kα radiation (λ = 1.5406 A°). The crystallite sizes were determined using the Scherrer formula $t = 0.9\lambda/\beta\cos\theta$, where λ is the wavelength characteristic of the Cu Kα radiation, b is the full width at half maximum (in radians) and is q the angle at which the 100 intensity peak appears.

Nitrogen adsorption isotherms were obtained by using Quantacrome Autosorb iQ and Asiqwin gas sorption system to find the surface area and their respective pore size distributions were obtained by BJH pore size distribution analysis. Morphology and elemental study were carried out by the SEM-EDAX analysis. Thermal studies were carried out on NETZSCH STA 409PC by using an Al_2O_3 crucible at the heating rate of 10 °C/min in oxygen atmosphere. TEM analyses were carried out to find the particle size of the synthesized catalyst on Phillips CM 200 operating voltages: 20-200 kV resolution: 2.4 A°. IR absorption spectra were recorded in the 4,000-400 cm^{-1} range on Shimadzu IR Prestige-21 by diluting a few milligrams of sample in KBr. PL measurements were performed using a Horiba Jobin Yuon Fluorolog 3 spectrophotometer equipped with a 450 W xenon lamp with a tunable excitation wavelength. Raman scatterings were recorded on Horiba JY Lab Raman HR 800 Micro Raman Spectrometer and excitation wavelength is 632.8 nm. Band gap determination is carried out by using a UV-VIS spectrophotometer (Shimadzu UV-2450).

ESR measurements were carried out on JEOL, Japan JES-FA200 ESR spectrometer. XPS spectra were recorded for the representative sample on a microtech multiple ESCA 3000 spectrometer.

The magnetic properties were measured on Quantachrome Versa Lab vibrating sample magnetometer (VSM) at 300 K.

TPD Analysis was carried out to measure the acidity of the samples using ammonia as a probe on a Chemisorb 2720, Micromeritics instrument. Typically, in a quartz tube, 100 mg of the sample (-100 mesh) was held between small lumps of inert quartz wool. The sample tube was connected to the device and heated to 120 °C, 12 h, to remove adsorbed water and other volatile impurities. After cooling to 25 °C, dry ammonia gas (20% NH_3, He (UHP); 20 mL/min) was then passed at for 15 minutes. The physically adsorbed ammonia was flushed out by He (UHP) carrier gas

at 25 °C. The sample was heated from 25 °C to 600 °C at a heating rate of 5 °C/min and the desorbed ammonia was measured using a thermal conductivity (TCD) detector.

2.2 *Photocatalytic activity*

2.2.1 *Photodegradation of methylene blue dye*

The photocatalytic activity was evaluated using methylene blue degradation as a test reaction. The experiment was carried out simultaneously for both catalysts in sunlight for 120 min, between 10.00 am and 12.00 noon. In a typical run, 100 mL of aqueous dye solution (12 ppm, pH = 7.5) and 0.4 g of the catalyst were taken in a 250 mL beaker and exposed to sunlight for the duration of the experiment. The pH was adjusted with 0.1 M NaOH solution. The solutions thus exposed to sunlight were stirred intermittently. After every 15 min 0.5 mL aliquots were pipetted out, centrifuged and the absorbance of the clear supernatants was determined at 660 nm wavelength against appropriate blanks.

2.2.2 *Photodegradation of 4-Nitrophenol*

Photocatalytic degradation of 4-Nitrophenol (4-Np) was carried out for all catalysts (0.01 g) in 50 mL of 0.1 mmol/L 4-Np in the presence of 5 mL of 0.1 M H_2O_2 (pH = 5). The solutions were exposed to sunlight. The solutions thus exposed to sunlight were stirred intermittently. After every 20 min 2 mL of the reaction mixture was centrifuged and the clear solution obtained was taken in the cuvette and analyzed by UV-Vis spectroscopy against an appropriate blank in the range of wavelength of 200-800 nm.

2.2.3 *Photooxidation of benzene to phenol*

Photocatalytic oxidation reactions were conducted in a quartz RB flask for different periods of time with a 400 W mercury lamp (λ = 200-400 nm) using a flow-type double-jacketed quartz reactor. In a typical experiment, 30 mg of catalyst was added to a reactant mixture of 2 mL of CH_3CN, 1 mL of benzene, and 2 mL of 25% H_2O_2. The temperature of the double-jacketed reactor and quartz RB was maintained at 25 °C by allowing water circulation. Before any irradiation, the reaction mixture was stirred for 30 min in the dark and irradiation was conducted for time between 5 to 18 h. After irradiation, organic and aqueous layers were separated with a separating funnel. Oxidized products of benzene were analyzed with an Agilent 6890 gas chromatograph (GC) equipped with a flame ionization detector (FID) and an HP-5.5% phenyl methyl siloxane capillary column. The presence of phenol was confirmed by analyzing both organic and aqueous layers.

3. Results and discussion

3.1 *Structure, surface and morphology study*

Several methods for the preparation of TiO_2 are reported most of them belong to the wet chemical methods. Among others wet chemical method hydrothermal and sol-gel method can be selected as the best method. Sol-gel method is a simple economical and most frequently used method that gives TiO_2 interesting properties such as different morphologies, small particle size and high surface area.[13-15] In the present investigation synthesis of TiO_2 catalyst was carried out by using hydrazine sulphate as fuel during the synthesis. Figure 1 shows the XRD pattern of synthesized samples T, T1 and T2. All the samples were calcined at 600 °C as seen from the TG curve in Figure 2 complete desulphation and samples attain stability at a temperature 600 °C. All the samples showed diffraction peaks associated with the tetragonal anatase phase of TiO_2 (JCPDS-782486). As seen in Figure 1 change in the ratio of titanium isopropoxide to hydrazine sulphate has slightly affected the crystallization of the titania. In the case of sample T and T1 peak broadening is observed then the T2 sample. The observed decrease in the peak intensity in T and T1 then the T2 signifies the amorphous nature of the samples. peak broadening indicates that particles were in the nanosize. For the nanosize powders XRD peak broadening is observed due to insufficient diffraction planes cancels the intensity outside the peak centers.

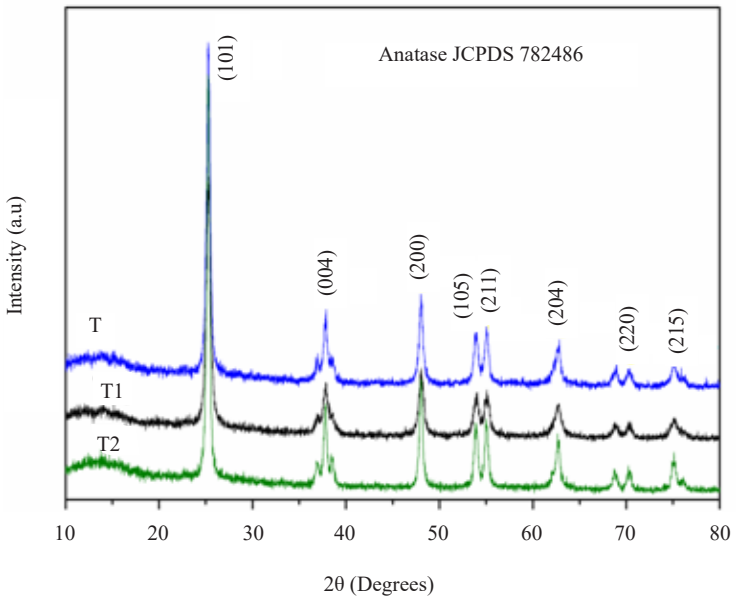

Figure 1. XRD pattern of the synthesized samples

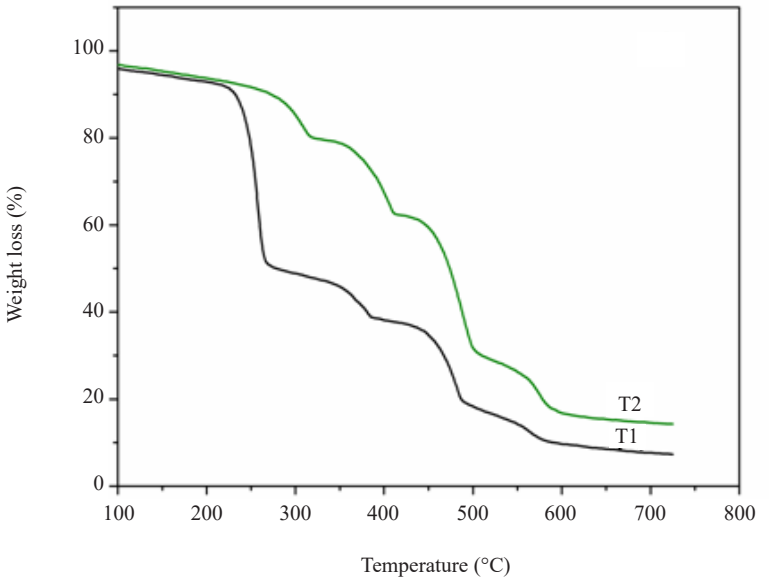

Figure 2. TG curves of the synthesized precursors

It is well known particle sizes play an important role and are affected when the fuel is used during the synthesis. Figure 3 shows TEM images of the synthesized samples. All the synthesized samples show samples with particle size in the nanometer range and are spherical in shape. Calculated particle sizes of the synthesized samples are given in Table 1.

TiO_2 samples were investigated by N_2 adsorption-desorption isotherms. Figure 4 (a) and (b) show the obtained results analyzed by the BET method for the surface area and BJH pore size distribution. The relative isotherms of the samples were of type IV, which is characteristic of mesoporous materials. The respective surface area values are given in Table 1. Samples are seen to have with high surface area and pore radius, which ensure enhanced reaction rates due to the high level of interaction of the reactant with the active sites.

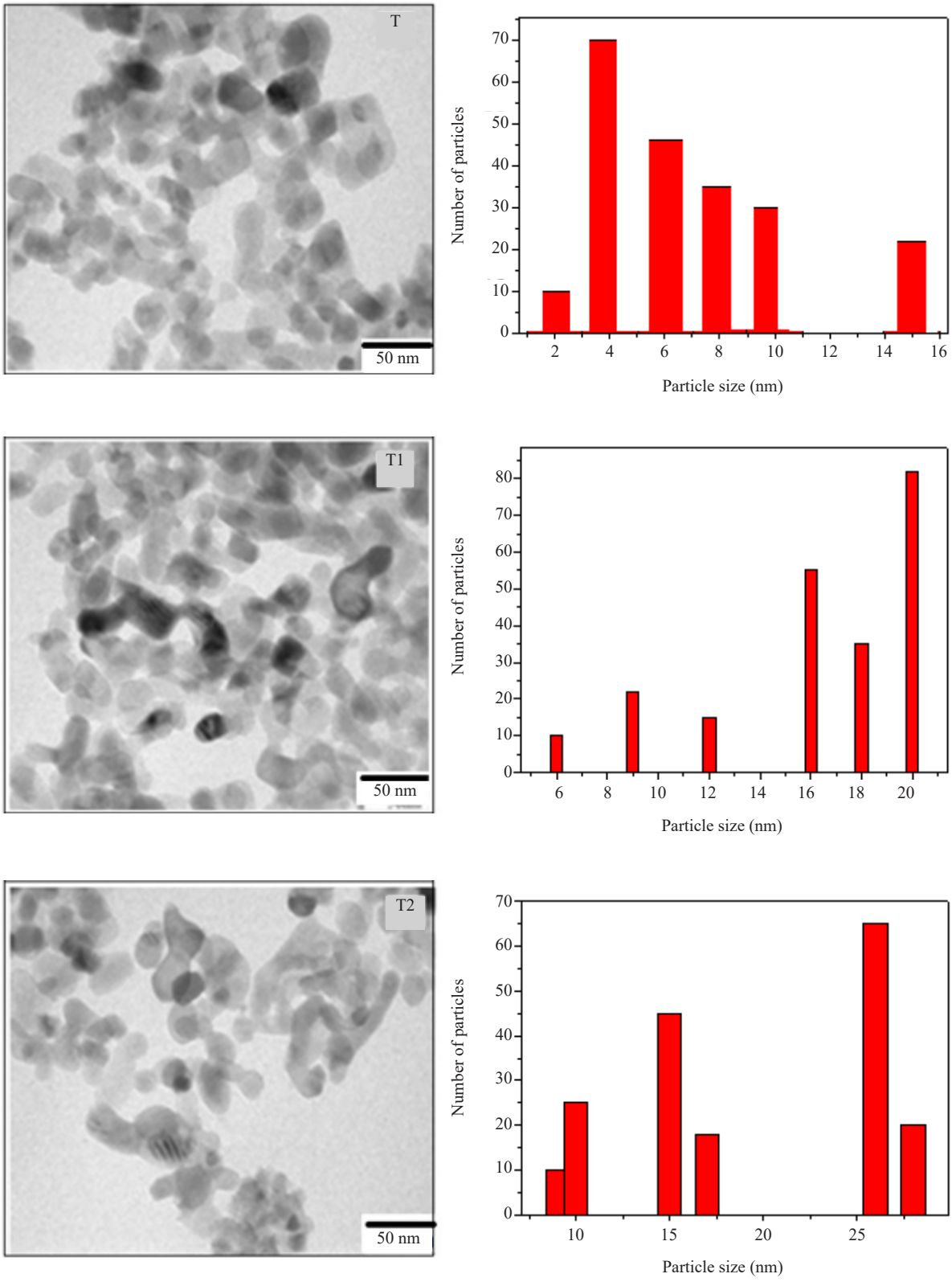

Figure 3. TEM images of the synthesized T, T1 and T2 samples with the respective hystographs

Table 1. Synthesis and properties of TiO_2 samples

Catalyst code	TEM particle sizes (nm)	Surface area (m^2/g)	Pore volume (cc/g)	Pore radius (Å)	Elemental data from EDAX analysis					Band gap (eV)
					Ti	O	S	O/Ti	S/Ti	
T	8	46	0.181	79.20	32.46	66.89	0.66	2.060	0.020	3.53
T1	14	47	0.202	86.55	32.61	66.85	0.54	2.049	0.016	3.49
T2	18	56	0.268	96.67	32.72	66.82	0.46	2.042	0.014	3.58

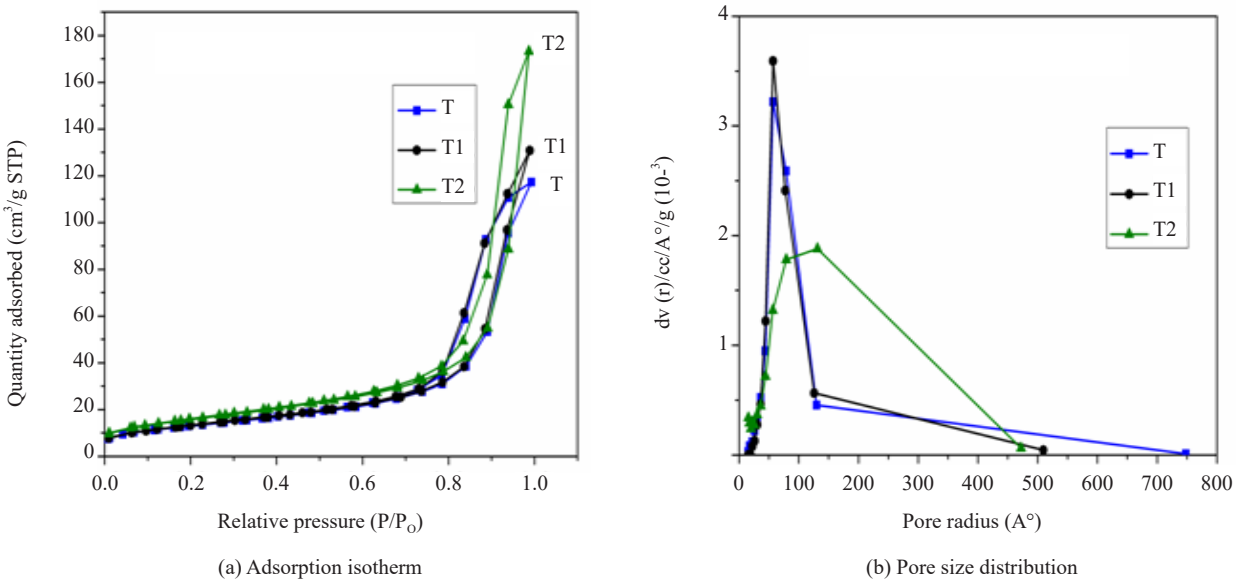

(a) Adsorption isotherm (b) Pore size distribution

Figure 4. (a) N_2 adsorption-desorption isotherm, (b) Pore size distributions of synthesized samples

The surface morphology of the samples is studied by scanning electron microscopy and micrographs are given in Figure 5. The samples appeared to be agglomeration of the smaller particles. The surface of the particles is rough and a large number of pores are found to be seen. The elemental data of the respective samples are given in Table 1. The presence of sulphur element peak was observed other than the Ti and O. It is seen that as the surface area increases, there is a decrease in the O/Ti ratio. The decrease in the O/Ti ratio indicates that there is a large number of surface defects present in the samples. These defects could be either cationic or anionic vacancies.

3.2 *Spectroscopic study*

Figure 6 shows Raman spectra of the synthesized TiO_2. As seen in the figure Raman spectra show six bands at Eg (1) → 142.8 cm^{-1}, Eg (2) → 197.6 cm^{-1}, B1g → 396.15 cm^{-1}, A1g + B1g → 514.8 cm^{-1}, Eg (3) → 639.7 cm^{-1}. The absence of the weak band around 140 cm^{-1} demonstrates that no rutile phase was present in the synthesized samples. There was also no band seen in a range of around 1,000 cm^{-1} which corresponds to the presence of the sulphate groups. Figure 6 inset depicts that Eg (1) signal is broad in T and T1 then the T2 and becomes intense. Raman signal of TiO_2 is very sensitive to the vibrational mode of O^{2-} ions in the Ti-O bond [19-20]. The strength of the Raman signal depends upon the polazibility of O^{2-} surrounding Ti^{4+} ion in the basic TiO_6 unit. The presence of oxygen vacancies will affect the vibration of the Ti-O bond and thus affect the intensity, position and width of the Raman bands. It is seen from the

Raman intensity of T2 is very low and the inset shows normalized spectra of the samples. From the normalized spectra, it is seen that Eg (1) band of T and T1 are more highly intense, broad and slightly blue-shifted than the T2 sample. This shift in the position and peak broadening signify the presence of oxygen vacancies in the TiO_2 octahedra.

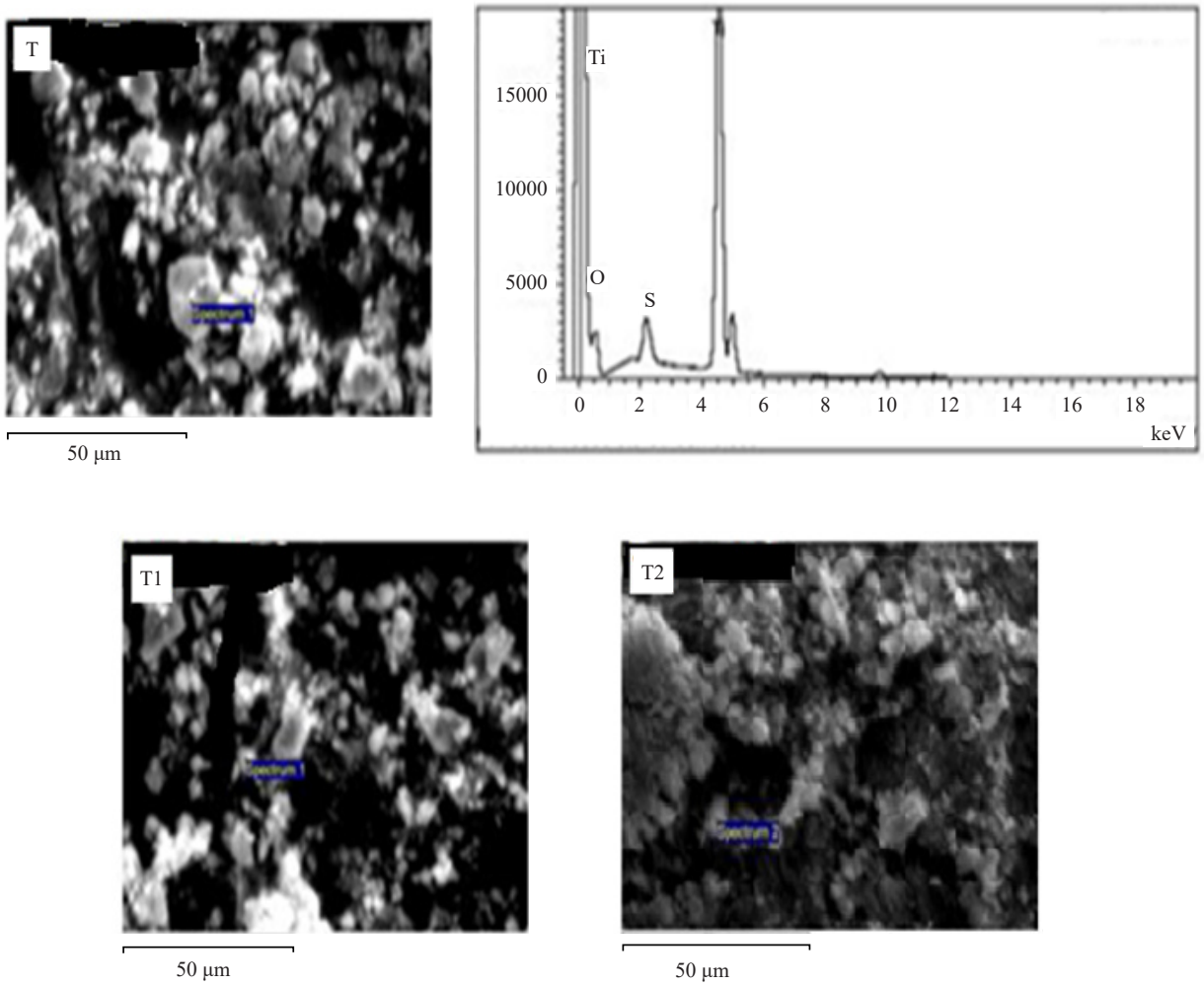

Figure 5. SEM-EDAX images of the synthesized samples

Figure 7 shows a peak in the samples at around 3,300-3,500 cm^{-1} due to stretching vibrations of O-H and bending vibrations of adsorbed water molecules. All the samples present spectra with strong bands located at around 700 cm^{-1} attributed to Ti-O stretching and Ti-O-Ti bridging stretching modes. The peak at around 1,640 cm^{-1} corresponds to bending vibrations of the O-H and N-H. The bands are seen in the range of 1,000 to 1,400 cm^{-1} in the T, T1, T2 and are absent in the DP-25. The presence of these bands could be due to S-O bond. This confirms our argument that the N and S doped TiO_2 is formed. Figure 6 inset gives a high resolution of the bands in the range from 400 to 700 cm^{-1}. The original vibration band in TiO_2 at 476 cm^{-1} is blue shifted to 482 cm^{-1} and vibrational modes at 574 cm^{-1} and 708 cm^{-1} are red shifted to 563 cm^{-1} and 689 cm^{-1}.

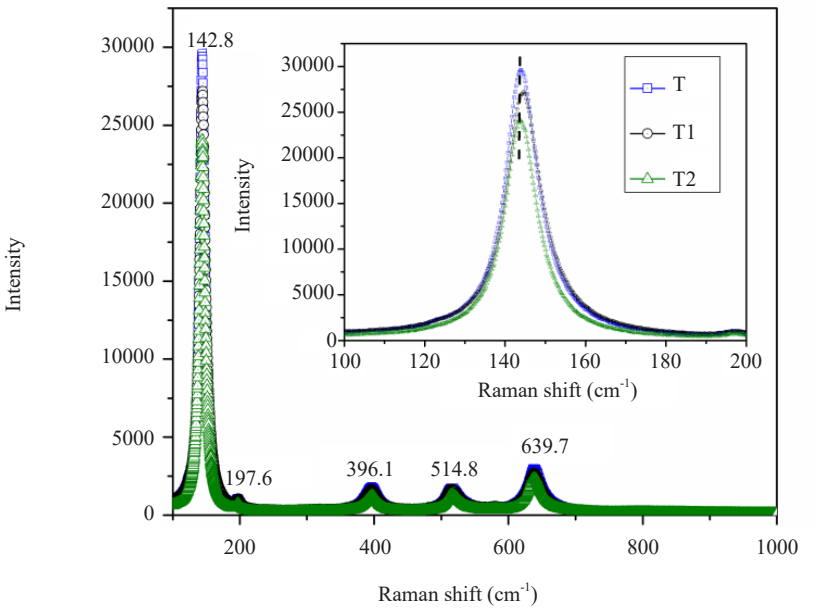

Figure 6. Raman spectra of synthesized samples

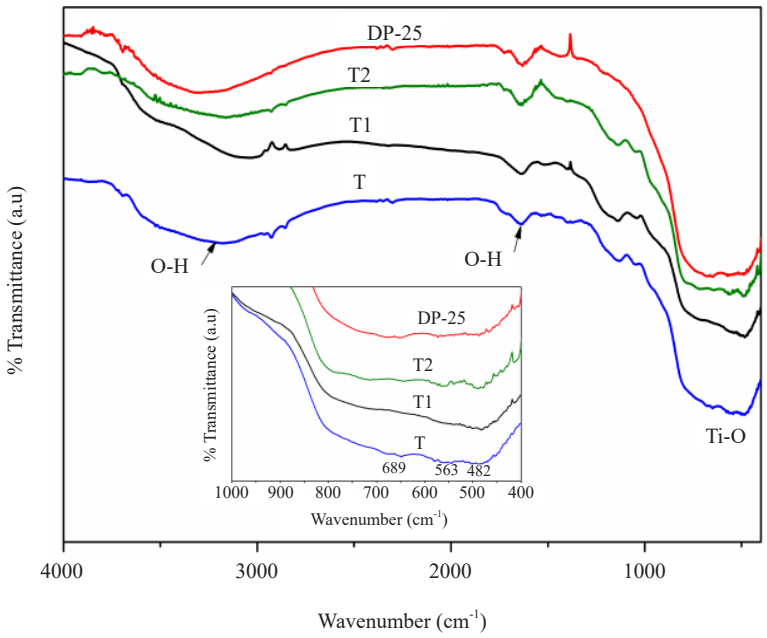

Figure 7. FTIR spectra of synthesized samples

Presence of sulphur in the synthesized catalyst were confirmed from SEM-EDAX analysis and the respective quantities of Ti, O and S are given in Table 1. As seen in Table 1 decrease in the O/Ti ratio indicates a deficiency in oxygen i.e. more oxygen vacancies in T2. The oxygen vacancies are generally created by the elimination of sulphate and OH functional groups elimination during the synthesis. ESR is a powerful tool for detecting the spin-polarized change state of defective TiO_2 nanostructure. ESR analysis was carried out to detect Ti^{3+}. Figure 8. gives ESR spectra of the synthesized TiO_2 samples. The presence of ESR signal at 2.003 is due to O^- whereas the signal at 1.980 is due to the presence of Ti^{3+} [16-18] presence of the peak at 2.003 in T, T1and T2 is due to Ti^{4+}-O_2^- superoxide species which is a result

of chemisorbed bonding of O_2 with Ti^{3+} centers.[17-18] In order to investigate the chemical state of the possible dopants into the TiO_2 lattice, XPS measurements are carried out and the binding energies of the Ti2p, O1s, N1s, and S2p are studied. The results obtained with peak positions are shown in Figure 9. According to the literature standards binding energy of $Ti2p_{3/2}$ in TiO_2, for Ti^{3+} is located at 457.7 eV and for Ti^{4+} is located at 459.5 eV. All the peak positions with respect to their binding energies are shifted towards higher values. This could be due to the presence of defects in the lattice. The high- resolution spectra show two peak at 458 eV and 464 eV and these two peaks are due to the presence of Ti^{3+} and Ti^{4+} in the samples. The binding energies for the $Ti2p_{3/2}$ and $Ti2p_{1/2}$ appeared at 464 eV and 469 eV respectively. This result shows that Ti^{4+} ions near oxygen vacancies occupy an electron from the oxygen vacancy cavity Vo and transform to Ti^{3+} ions yielding an F^+ center. An increased intensity of Ti^{3+} strongly indicates the presence of a high concentration of oxygen vacancies which are created during the synthesis process as compared to DP-25. Also shift in the peak position towards higher binding energy in T, T1 and T2 was observed as compared to DP-25 could be due to nitrogen and sulphur doping. Figure 9 (d) shows O1s spectra for the samples T, T1, T2 and DP-25. The O1s peak for the samples appeared at around 528 eV. The existence of O1s spectra asymmetric curve at high binding energy indicates that several oxygen species are present in the near-surface region[19-22] Figure 9 (c) shows the peak at 397 eV which is due to the existence of nitrogen doping into the TiO_2 lattice. Figure 9 (b) shows the peak at 168-169 eV corresponding to the sulphur binding energies. Therefore from the figure, it is clear that sulphur was doped into the lattice. The presence of Ti^{3+}, N, and S was therefore confirmed from the XPS studies.

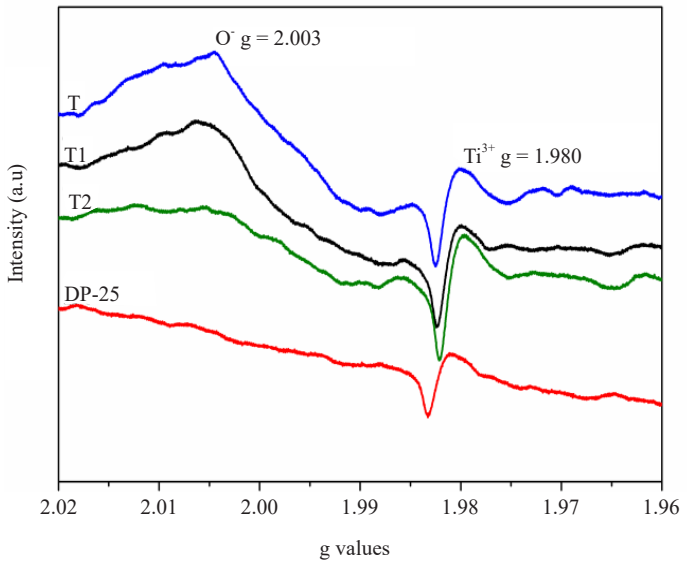

Figure 8. ESR spectra of synthesized TiO_2 samples

Figure 10 shows the UV-Vis spectra of the synthesized samples. All the samples show absorbance at 350-400 nm with a shift towards the visible region. The red shift in the samples could be due to the presence of Ti^{3+} in the octahedral lattice of TiO_2 and is confirmed by the ESR and XPS studies. From the XPS studies, it was also confirmed that there is the presence of nitrogen and sulphur in the T, T1 and T2 samples and is absent in the DP-25. Whereas Ti^{3+} is present in all the samples including DP-25. Therefore red shift of DP-25 is due to the presence of Ti^{3+} and red shift in T, T1 and T2 then the DP-25 is due to the presence of nitrogen and sulphur doping taking place into the lattice.[19-22] Photoluminescence is a result of surface phenomenon and a change in the surface environment would have a significant effect on the photoluminescence scan process. Large surface area and strong presence of defect, the effect of defect-related PL emission is strong. Figure 11 shows PL spectra for the synthesized samples. All the samples show an emission peak at 370-390 nm corresponding to the phonon-assisted indirect L → M transition from the conduction band edge to the valence band in the Brillouin zone.[19-23] The emission peak originating in the wavelength range between 400-800 nm

is usually associated with self-trapped excitons, oxygen vacancies and surface defects. Visible luminescence bands originate in the TiO_2 mainly due to the oxygen vacancies with Ti^{3+}.

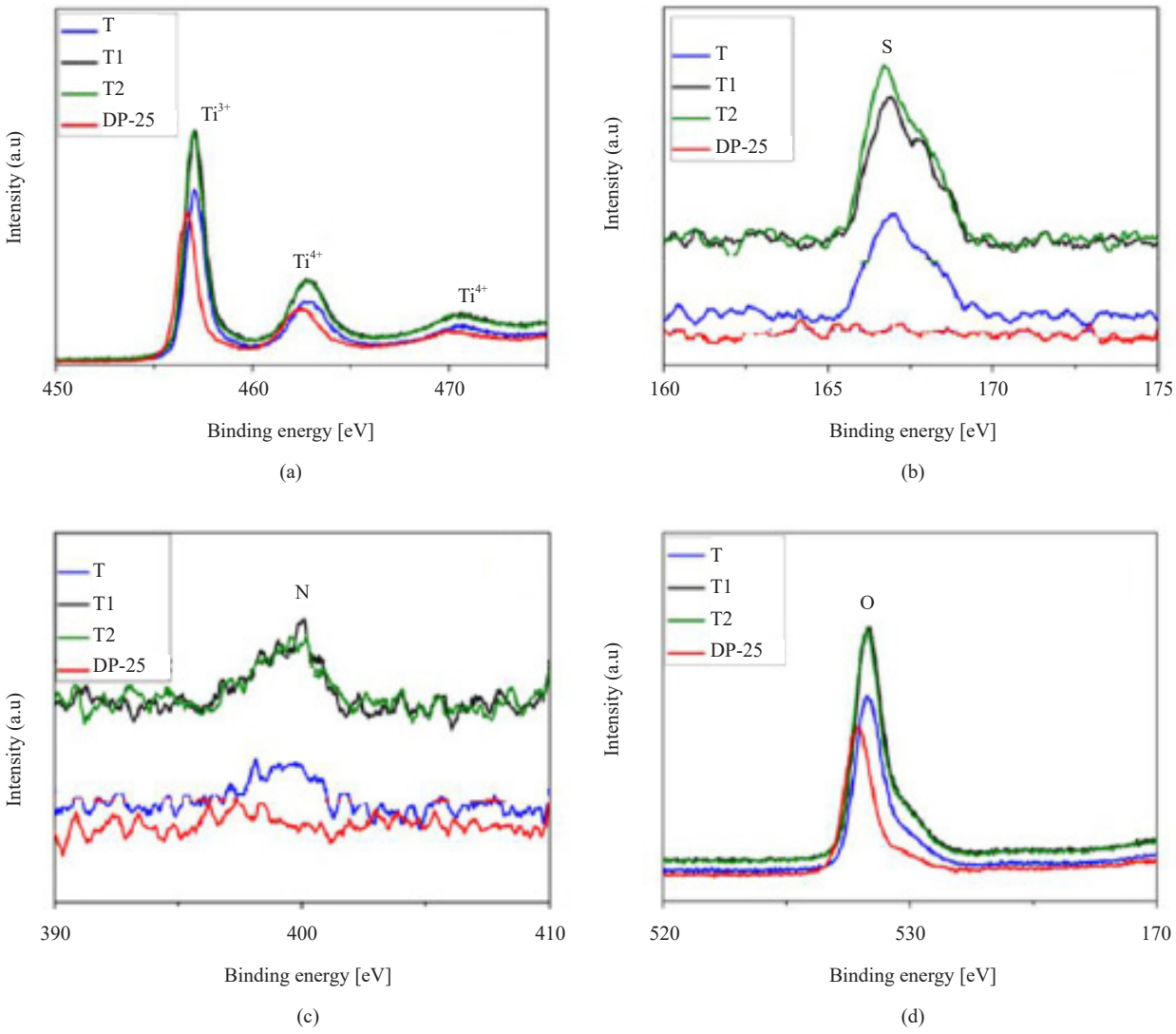

Figure 9. XPS of T, T1, T2 and DP-25 samples (a) Ti2p (b) S2p (c) N1s (d) O1s

The presence of oxygen vacancies is confirmed by the earlier characterized techniques. The presence of oxygen vacancies is mainly considered as F centers. Most of the surface and grain boundary oxygen vacancies act as non-radiative centers and therefore PL spectra is seen to be less intense. The intensity of bands was higher in the case of T than those of other samples and this could be due to the large number of N and S doping in the T than other samples.The presence of oxygen defects results in occupying position below the conduction band at a level of 0.7 to 1.0 eV, which further result in electrons taking a longer time to recombine with the holes resulting in the PL spectra with less emission intensity. Whereas nitrogen and sulphur doping will occupy a level just above the valence band and will inhibit the facile recombination of the electron and hole. Therefore from the above spectra it can be seen that high-intensity peaks are due to the presence of nitrogen and sulphur doping whereas reduction in the peak emission intensity takes place due to oxygen vacancies. Thus PL analysis evidence that there is the presence of oxygen vacancies and nitrogen and sulphur doping in the synthesized samples.

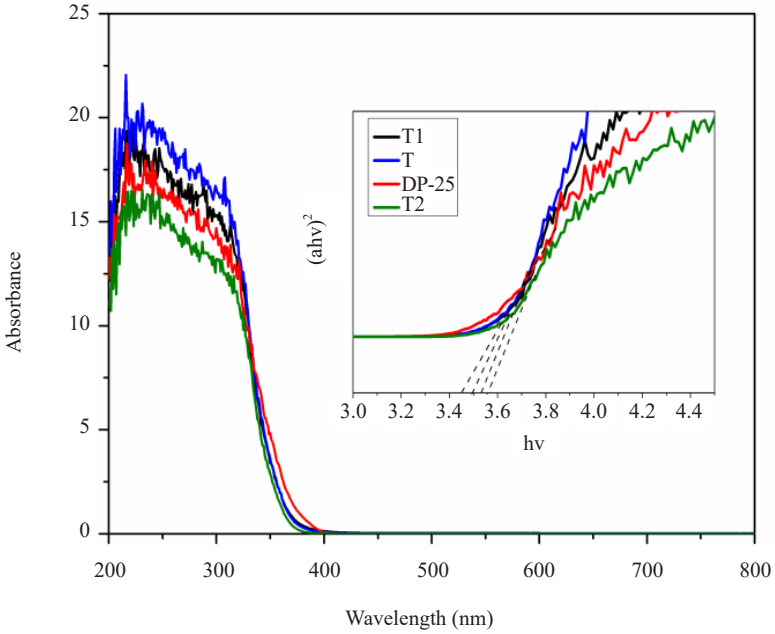

Figure 10. UV-Vis spectra of the synthesized samples

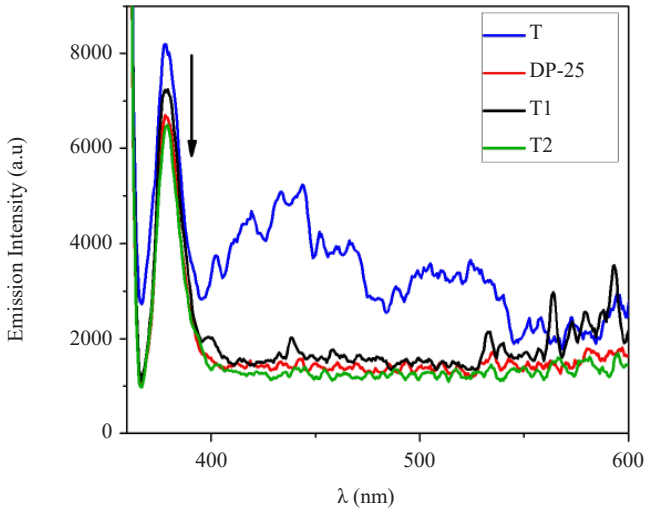

Figure 11. Photoluminscence spectra of the samples

3.3 *Surface acidity*

Raman analysis predicts the presence of defects in the samples and IR, SEM-EDAX, and ESR analysis gives evidence for the presence of oxygen vacancies due to shifts in bond vibration modes and elimination of sulphate and decrease in O/Ti causing a defect in the samples. In order to study the type of acid strength pyridine adsorption was carried out on the synthesized samples. After pyridine adsorption samples showed bands at 1,600 cm^{-1} and 1,402 cm^{-1} and are associated with is Lewis acid site as shown in Figure 12 (b).[24] There were no bands seen due to the presence of Bronsted acid sites. This could be due to a lack of OH groups. pyridine adsorbed IR spectra shows the presence of Lewis acidity in the all synthesized samples. In order to know the amount of acid sites NH_3-TPD analysis was carried out. The results of the NH_3-TPD are given in the Figure 12 (a). Table 2 gives the amount of acidic sites on the synthesized

TiO_2 samples T and T1 show high acid values as compared to T2. ESR and XPS spectroscopy confirmed the presence of Ti^{3+} and nitrogen and sulphur doping in the samples in comparison to the DP-25. Lewis acidity originated due to the presence of Ti^{4+} and Ti^{3+} in the samples. T2 shows only medium-strength acid sites due to the presence of less quantity of Lewis acid sites whereas in the case of T1 and T there is the presence of both weak and medium type acidity and are found to be highly acidic due to more Lewis acid sites. It is also stated by L. Xiong et al.[4] that TiO_2 surface with Ti^{3+} will give a lower acidic value in TPD profile than the Ti^{4+}, due to the strong binding of Ti^{3+} site. Therefore from the 10 a) one can conclude that the T2 with low acidic value is due to the presence of more Ti^{3+} and high oxygen vacancies.

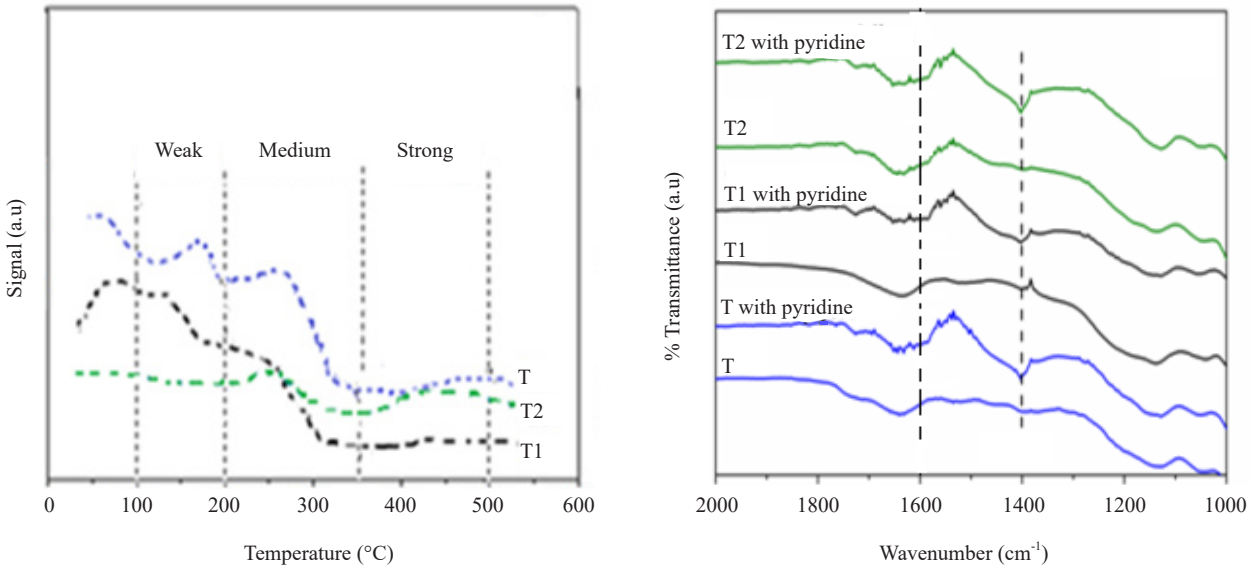

Figure 12. (a) NH_3-TPD profile for synthesized samples and (b) IR of pyridine adsorbed on samples

Table 2. NH_3-TPD data of synthesised samples

Catalyst code	Strength of acid sites (mol·g^{-1})			Total acidity	
	Weak (100 °C-250 °C)	Medium (250 °C-350 °C)	Strong (3500 °C-450 °C)	(W + M + S) (mol/g)	(M + S) (mol/g)
T	36	36	18	90	54
T1	36	20	0	66	30
T2	6	12	18	36	30

3.4 *Magnetic measurement*

Magnetic measurements of the synthesized samples were carried out using VSM. Figure 13 gives hysteresis loop profiles of the synthesized samples and also compared with Degussa (DP-25). Ferromagnetic property in the metal oxide depends on the shape, size and porosity of the catalyst.[21] Sample T2 shows magnetism up to 0.07 emu/g given in Table 3 and this magnetism in T2 could be due to high particle size, porosity and presence of oxygen vacancies. A catalyst with high porosity is obtained when there is a sudden increase in calcinations temperature or at high temperature and this takes place due to the elimination of organic matter or water molecules. When such a process occurs it develops porosity

and defects or vacancies. T2 is highly porous with a high surface area of 55.99 m^2/g and oxygen vacancies as seen from the IR, Raman, UV and EDAX analysis. The presence of oxygen vacancies is the reason for high magnetic moment in T2 and T1, T shows a lower magnetic moment compared to T2 but in the case of DP-25 magnetism is high compared to T1. This could be due to the existence of mixed phases in commercial DP-25 catalysts. The respective magnetic values are given in Table 3. The presence of vacancies changes the band structure by occupying localized Ti 3d orbit and thus reduces Ti^{4+} to Ti^{3+} ions and F^+ centre formed. s-d exchange interaction between F^+ centre and Ti^{3+} favors the existence of ferromagnetism in TiO_2 as the presence of Ti^{3+} is evident from the XPS results.[16] In the present study, it is seen that the ferromagnetism exists because of oxygen vacancies, high surface area and porosity of the catalyst. The existence of ferromagnetism is due to both oxygen vacancy and porosity which further improves the visible light activity of the catalyst and such catalyst could be well suitable for photocatalysis and spintronics.

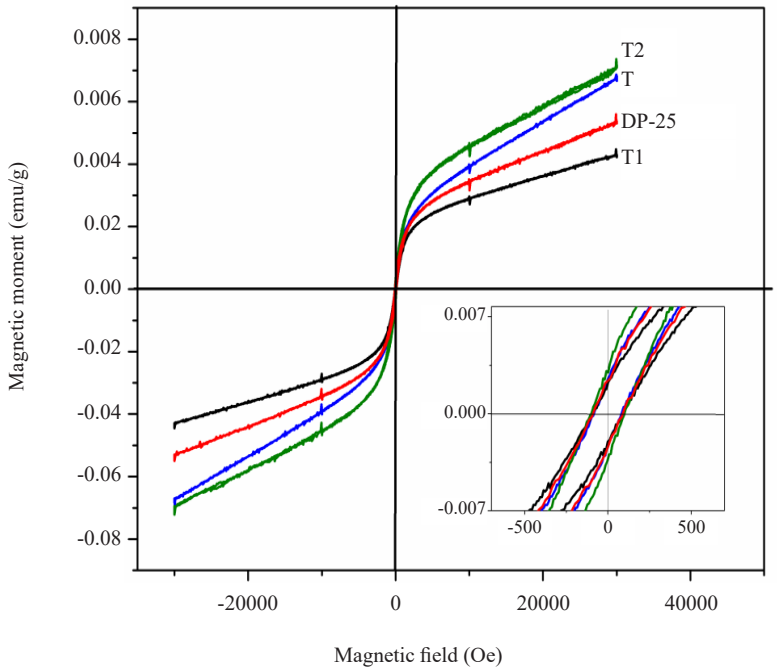

Figure 13. VSM analysis of T, T1, T2 and DP-25

Table 3. Magnetic properties of the samples

Catalyst code	Magnetic properties		
	Ms (emu/g)	Mr (emu/g)	Hc (Oe)
T	0.067	0.002	79.85
T1	0.043	0.002	89.81
T2	0.071	0.002	98.81
DP-25	0.053	0.002	89.81

4. Effect of surface properties on the photocatalytic activity of N-S doped TiO_2 with oxygen vacancies

From the results of various characterization techniques and NH_3-TPD profiles, it is seen that T2 catalyst possesses more number of oxygen defects of oxygen vacancies, whereas catalyst T1 and T possesses more surface acidity. The photocatalytic activity of all the synthesized catalyst was evaluated for the photodegradation of methylene blue dye and 4-Nitrophenol as pollutants.

Compared to commercial TiO_2 i.e. DP-25 the synthesized catalyst T2, T1 and T showed higher and more competitive photocatalytic activity. The higher activity shown by catalyst T2 could be due to the presence of surface oxygen defects and high surface area. Similarly high activity in T and T1 catalyst could be due to its small particle size and acidic nature. In metal oxide presence of oxygen vacancies will act as an electron trapping site which further inhibits the electron-hole recombination. Oxygen vacancies in metal oxides will occupy the level below the conduction band and thus trap the electron which leads to inhibition of the electron hole pair recombination process.

In the case of the catalyst with a higher surface area process of adsorption onto the surface of the catalyst is more facile. The higher the adsorption high will be the activity of photocatalytic result. In the case of catalysts T1 and T presence of Lewis acidity will help in O_2 adsorption process wherein further helps trap electrons in the photocatalytic process.

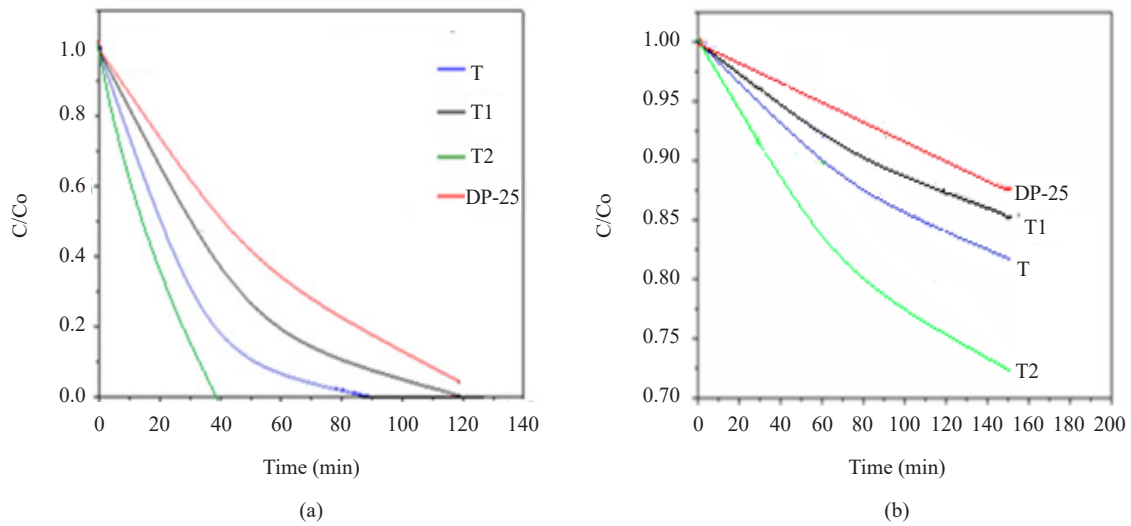

Figure 14. Photodegradation of methylene blue dye and of 4-Nitrophenol

Lewis acidity in the samples helps in the chemisorptions of water to generate reactive hydroxyl radicals which further enhance the rate of photocatalysis. Whereas, adsorption of oxygen is more predominant on the oxygen-deficient surface thus facilitating interfacial charge transfer.[24] The high activity of T, T1 and T2 than the DP-25 could be also due to nitrogen and sulphur doping as evident from XPS studies. As seen in the Figure 14.

All three catalysts were N and S doped and showed higher photocatalytic activity than DP-25 therefore one of the catalysts T with 1:3 molar ratio of titanium isopropoxide and hydrazine sulphate and with small particle size was further studied for photooxidation of benzene to phenol reaction. The results of the photooxidation of benzene to phenol is summarized in Table 4. The photocatalytic activity was measured at different time intervals under UV irradiation. The results show that after irradiation of 20 h. T showed 11.8% of the benzene conversion with 86% selectivity. The level of benzene conversion increases as the irradiation time increases from 5 to 20 h, respectively, a decrease in the phenol selectivity was also observed from 100% to 86%. The decrease in the phenol selectivity is mainly due to further oxidation of phenol to other side products, such as hydroquinone. Many control experiments were also conducted, such

as benzene oxidation without a catalyst. In the dark or without irradiation, there is not much reaction. Irradiation for 20 h without a catalyst induces the photochemical oxidation of benzene. A large amount of side products were observed in the case of without catalysts, indicating the presence of free radicals which enhances the free radical mechanism due to photochemical conversion and homogeneous cleavage of hydrogen peroxide decomposition. The high benzene conversion was observed in the case of UV irradiation than the visible light thus facilitating the necessary of the energetic holes on the titania surface. Without hydrogen peroxide there was no conversion of benzene was observed therefore highlighting the role of dissolved oxygen thus the pathway of green chemistry.

Comparative study between DP-25 and synthesised catalyst T shows that T gives a higher % conversion of benzene than the DP-25. As from the XPS data DP-25 is N doped and T is N and S doped thus indicating that additional sulphur doping enhances the % conversion of the benzene this could be due to different energy levels of the N and S in the TiO_2.

Table 4. Photocatalytic benzene to phenol oxidation measured under different conditions

Catalyst and irradiation conditions	t (h)	Benzene conversion (%)	Phenol	
			Yield (%)	Selectivity (%)
Without catalyst	5	0.25	0.25	100
DP-25 (UV)	5	0.83	0.78	94.19
T (UV)	5	1.13	1.13	100
T (Visible)	5	0.3	0.3	100
T (UV)	15	9.1	9.1	100
T (UV)	20	11.8	10.2	86
T (no light)	20	2.0	2.0	100
Without catalyst	20	1.2	0.6	50

4.1 *Possible photocatalytic mechanism*

Possible general mechanism for the photocatalytic oxidation of benzene to phenol is shown in Figure 15. Synthesis TiO_2 was found to be with both nitrogens as well as sulphur doping. In such case nitrogen in the TiO_2 will occupy the energy level just above the valence band of the TiO_2 and sulphur will occupy the energy level just below the conduction band of the TiO_2. TiO_2 with the pure anatase form is found to have with band gap value of around 3.2 eV. The simultaneous presence of the sulphur and nitrogen in the TiO_2 will reduce the band gap of the TiO_2 to ~2.7 eV which is convenient for the absorption of visible light. During the photocatalytic oxidation conversion of the benzene to phenol holes in the valence band will move to the CB and will then travel to the energy level of the sulphur thus inhibiting the electron-hole pair recombination and increasing the photocatalytic activity. When the catalyst is irradiated with the light maximum holes present in the valence band of the photocatalysts will undergo the oxidation process of the benzene forming benzene radical ions. Benzene radical ions will further react with the hydroxyl radicals forming phenol. However, because of the presence of Schottky junctions which is due to the presence of sulphur doping, the transfer of the electron from the CB to S can also trap the electrons for any reduction reactions on S energy levels. Thus presence of both S and N doping will facilitate the absorption of the visible light and will also facilitate the oxidation process to the maximum conversion of the phenol product.

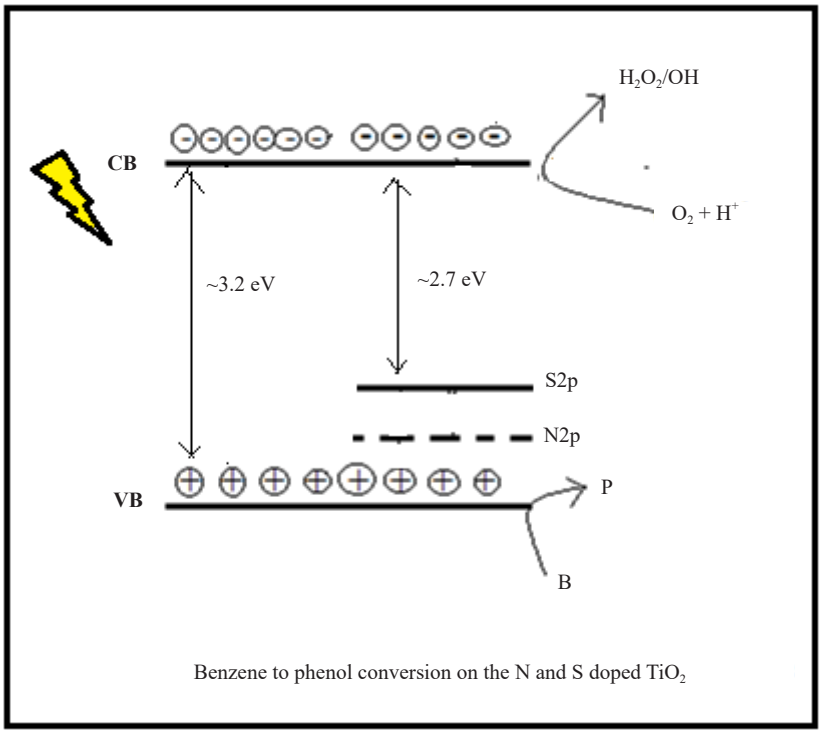

Figure 15. Possible general mechanism of the benzene to phenol conversion on the S and N doped TiO_2

5. Conclusions

Synthesis of TiO_2 was carried out using hydrazine sulphate as fuel. Synthesized TiO_2 was found to be with smaller particle size and high surface area confirmed form the TEM and BET analysis. SEM-EDAX elemental analysis, Raman and PL spectra showed the presence of oxygen vacancies in the TiO_2 samples. From the ESR and XPS studies, it was seen that there is the presence of Ti^{3+}. XPS also showed that there is nitrogen and sulphur doping occurred in the synthesized TiO_2 samples. The acidic nature of the synthesized TiO_2 was confirmed by the NH_3-TPD profiles. Our results provide convincing evidence for the occurrence of room-temperature ferromagnetism in the TiO_2 samples. Synthesized TiO_2 catalyst shows high photodegradation activity for methylene blue dye then the DP-25 catalyst. T synthesized catalyst showed high activity for the photocatalytic oxidation of benzene to phenol than the DP-25.

Acknowledgement

The authors are grateful for financial support from the University Grants Commission, (UGC-SAP) New Delhi and UGC-BSR/Fellowship/2014/1512.

Conflict of interest

The authors declare no competing financial interest.

References

[1] Li, X.; Zou, M.; Wang, Y. Soft-template synthesis of mesoporous anatase TiO_2 nanospheres and its enhanced

photoactivity. *Molecules*. **2017,** *22*, 1943.
[2] Papp, J.; Soled, S.; Dweight, K.; Wold, A. Surface acidity and photocatalytic activity of TiO_2, WO_3/TiO_2, and MoO_3/TiO_2 photocatalysts. *Chem. Mater*. **1994,** *6*, 496-500.
[3] Lin, X. H.; Li, S. F. Y. Elucidation of structures of surface sulfate species on sulfated titania and mechanism of improved activity. *J. Appl. Cat. B: Env*. **2017,** *203*, 731-739.
[4] Xiong, L. B.; Li, J. L.; Yang, B.; Yu, Y. Ti^{3+} in the surface of titanium dioxide: Generation, properties and photocatalytic application. *J. Nanomater.* **2012,** *831524*, 13.
[5] Colon, G.; Hidalgo, M. C.; Munuera, G.; Ferino, I.; Cutrufello, M. G.; Navia, J. A. Structural and surface approach to the enhanced photocatalytic activity of sulfated TiO_2 photocatalyst. *J. Appl. Catal. B: Env*. **2006,** *63*, 45-59.
[6] Parrino, F.; Pomolla, F. Titanium dioxide and its applications. *J. Metal Oxides*. **2021,** 13-66.
[7] Gandhe, A. R.; Naik, S. P.; Fernandes, J. B. Selective synthesis of N-doped mesoporous TiO_2 phases having enhanced photocatalytic activity. *J. Micro. and Meso. Mat*. **2005,** *87*, 103-109.
[8] Gandhe, A. R.; Fernandes, J. B. A simple method to synthesize N-doped rutile titania with enhanced photocatalytic activity in sunlight. *J. of Solid State Chem*. **2005,** *178*, 2953-2957.
[9] Hussain, S. T.; Khan, K.; Hussain, R. Size control synthesis of sulfur doped titanium dioxide (anatase) nanoparticles, its optical property and its photo catalytic reactivity for $CO_2 + H_2O$ conversion and phenol degradation. *J. Nat. Gas Eng*. **2009,** *18*, 383-391.
[10] Kim, D.; Hong, J.; Park, Y. R.; Kim, K. J. The origin of oxygen vacancy induced ferromagnetism in undoped TiO_2. *J. Phys: Condens. Matter*. **2009,** *21*, 195405.
[11] Ping, W.; Ying, Z.; Guang, X.; Di, M.; Ping, Q.; Xiaoxia, Z. Ti^{3+} self doped TiO_2 as a photocatalyst for cycloxehane oxidation under visible light irradiation. *J. Materiomics*. **2019,** *5*, 696-701.
[12] Wang, S.; Pan, L.; Song, J.; Mi, W.; Zou, J.; Wang, L. Titanium-defected undoped anatase TiO_2 with p-type conductivity, room-temperature ferromagnetism, and remarkable photocatalytic performance. *J. Am. Chem. Soc*. **2015,** *137*, 2975-2983.
[13] Liang, Y.; Sun, S.; Deng, T.; Ding, H.; Chen, W. The preparation of TiO_2 film by the sol-gel method and eavlution of its self cleaning property. *J. Materials*. **2018,** *11*, 450.
[14] Choudhury, B.; Choudhury, A. Room temperature ferromagnetism in defective TiO_2 nanoparticles: Role of surface and grain boundary oxygen vacancies. *J. Mater. Sci. Eng. B*. **2013,** *178*, 239.
[15] Ohsaka, T.; Izunri, F.; Fujiki, Y. Photoluminescence and structural analysis of samarium doped TiO_2 thin films and their applications to visible LEDs. *J. Raman Spectroscopy*. **1978,** *7*, 321.
[16] Santara, B.; Giri, P. K.; Imakita, K.; Fujii, M. Evidence of oxygen vacancy induced room temperature ferromagnetism in solvothermally sythesised undoped TiO_2 nanoribbons. *J. Nanoscale*. **2013,** *5*, 5476-5488.
[17] Zhang, J.; Jin, Z.; Feng, C.; Yu, L. ESR study on the visible photocatalyst mechanism of nitrogen doped novel TiO_2: synergetic effect of two kinds of oxygen vacancies. *J. Solid State Chemistry*. **2011,** *184*, 3066-3073.
[18] Chang, S.; Hao, C.; Lo, P.; Chang, C. Preparation of phosphated Zr-doped TiO_2 exhibiting high photocatalytic activity through calcination of ligand-capped nanocrystals. *J. Appl. Cat. B: Env*. **2009,** *90*, 233-241.
[19] Erden, B.; Hunsicker, R.; Simmons, G.; Sudol, E.; Dimonia, V. XPS and FTIR surface characterization of TiO_2 particles used in polymer encapsulation. *Langmuir*. **2001,** *17*, 2664-2669.
[20] Bharti, B.; Kumar, S.; Kumar, R. Formation of oxygen vacancies and Ti^{3+} state in TiO_2 thin film and enhanced optical properties by air plasma treatment. *Sci. Rep*. **2016,** *6*, 32355.
[21] Pany, S.; Parida, K. M. Sulfate-anchored hierarchical meso-macroporous N-doped TiO_2: A novel photocatalyst for visible light H_2 evolution. *ACS Sustainable Chem. Eng*. **2014,** *2*, 1429-1438.
[22] Serpone, N.; Lawless, D.; Khairutdinov, R. Size effects on the photophysical properties of colloidal anatase TiO_2 particles: Size quantization versus direct transitions in this indirect semiconductor. *J. Phys. Chem*. **1995,** *99*, 16646.
[23] Li, H.; Vrinat, M.; Berhault, G.; Li, D. Hydrothermal synthesis and acidity characterization of TiO_2 polymorphs. *J. Materials Research Bulletin*. **2013,** *48*, 3374-3382.
[24] Lu, J.; Kosuda, K.; Duyne, R.; Stair, P. Surface acidity and properties of TiO_2/SiO_2 catalysts prepared by atomic layer deposition: UV-visible diffuse reflectance, DRIFTS and visible raman spectroscopy studies. *J. Phys. Chem. C*. **2009,** *113*, 12412-12418.